AIP Conference Proceedings

Shock/shock interference in hypersonic low-density flows near a cylinder

Cite as: AIP Conference Proceedings **2132**, 100003 (2019); https://doi.org/10.1063/1.5119598
Published Online: 05 August 2019

Vladimir V. Riabov, and Andrei V. Botin

View Online Export Citation

AIP Conference Proceedings
Get 30% off all print proceedings!
Enter Promotion Code PDF30 at checkout

AIP Publishing

© 2019 Author(s).

Shock/Shock Interference in Hypersonic Low-Density Flows near a Cylinder

Vladimir V. Riabov[1, a)] and Andrei V. Botin[2]

[1]*Department of Mathematics and Computer Science, Rivier University, 420 S. Main St., Nashua, NH 03060, USA*
[2] *Central Aero-Hydrodynamics Institute (TsAGI), Zhukovsky-3, Moscow Region 140180, Russia*

[a)]Corresponding author: vriabov@rivier.edu

Abstract. The interference of an impinging plane oblique shock wave with the viscous shock layer on a cylinder has been studied numerically for rarefied-gas flow regimes at the Reynolds numbers $15.5 \le Re_{R,0} \le 124$ and Knudsen numbers $0.1 \ge Kn_{R,\infty} \ge 0.012$. The calculations have been performed within the framework of the direct simulation Monte-Carlo technique [1] and the Navier-Stokes equations for a perfect gas using the shock capturing method [2]. The principal properties of flow parameters have been studied for five different types of interference at low Reynolds numbers. The differences with respect to the previously investigated interference regimes for high Reynolds numbers have been examined. The comparison analysis of numerical results and experimental data has been provided. It has been found that the local pressure and heat transfer coefficients on the surface of a cylinder may considerably (by a factor of 3.5) exceed the values on the edge stagnation line observed in the absence of interference. The type IV interference pattern observed in continuum flows has not been found in this study.

INTRODUCTION

The optimum flow rate through the air intake of a hypersonic vehicle occurs when the forebody oblique shock wave impinges on the blunt edge of the air intake [3, 4]. For hypersonic continuum flow conditions, six types of interference patterns between an impinging oblique shock and a viscous shock layer about a cylindrical blunt edge have been studied by Edney [5], Wieting and Holden [6], Borovoi [7], Borovoi et al. [8], Purpura et al. [9], and Tannehill et al. [10]. These studies indicate that the surface pressure and heat flux may considerably exceed the stagnation line values in the absence of interference. The rarefied hypersonic flow regimes have been analyzed in experiments of Botin [11], Pot et al. [12], and Riabov and Botin [13].

In the present study, the interference of an impinging shock with the viscous shock layer on a cylinder modeling a hypersonic inlet edge has been studied experimentally and numerically for rarefied flow regimes as characterized by Reynolds numbers $15.5 \le Re_{R,0} \le 124$ and Knudsen numbers $0.1 \ge Kn_{R,\infty} \ge 0.012$. The numerical results have been obtained by using the direct simulation Monte Carlo (DSMC) technique [14] and by solving the Navier-Stokes equations while employing a shock capturing method [15]. The DSMC-DS2G computer code [16] was developed by G. A. Bird. Results are compared with experimental data obtained in a vacuum wind tunnel by using the thermal sensitive coating technique [11, 17].

FLOW PATTERNS

We consider the interference of steady flow around an infinite circular cylinder and an impinging oblique shock in a hypersonic stream of rarefied air. The plane oblique shock with inclination angle β is generated by a wedge with an apex angle θ. The flow patterns over the cylinder had been discussed in detail by Edney [5], Borovoi [7], and Purpura et al. [9].

31st International Symposium on Rarefied Gas Dynamics
AIP Conf. Proc. 2132, 100003-1–100003-10; https://doi.org/10.1063/1.5119598
Published by AIP Publishing. 978-0-7354-1874-5/$30.00

Let us suppose that the oblique shock meets the bow shock ahead of a cylinder at different locations, thereby generating different interference type patterns:

a) Type I interference is characterized by the formation of two shocks after the intersection of two oblique shocks of opposite families. The intersection point is sufficiently downstream of the sonic point on the bow shock wave.
b) Type II interaction reflects the Mach phenomenon [5, 7-9] and produces two triple points separated by a normal shock after the intersection of the two oblique shock waves.
c) If the oblique shock crosses the strong bow shock, a slip line is produced separating subsonic area from a supersonic flow zone. In the type III interference case, the slip line reattaches on the body surface. This case would be only possible in continuum at small inclination angles, $\beta \leq 20$ deg. [5, 9].
d) If the slip line is unable to reattach on the wall, a supersonic jet, bounded by subsonic regions, develops (type IV) [5, 7]. The special case of a curved supersonic jet (type IVa) was studied by Purpura et al. [9].
e) Both weak oblique shock waves of the same direction would interact above the upper sonic line generating a supersonic jet after the upper multiple point (type V) [9].
f) Far from the leading critical point of the cylinder, a shock, a slip line and an expansion wave would be generated behind the triple point above the considered region (type VI) [7-9].

For continuum flows, the theory of shock polar [9, 12] can be effectively used to predict the localization of the different interference types around a cylinder. In the present study, a similar technique has been employed to estimate boundaries of interaction zones, as well as upstream boundary locations.

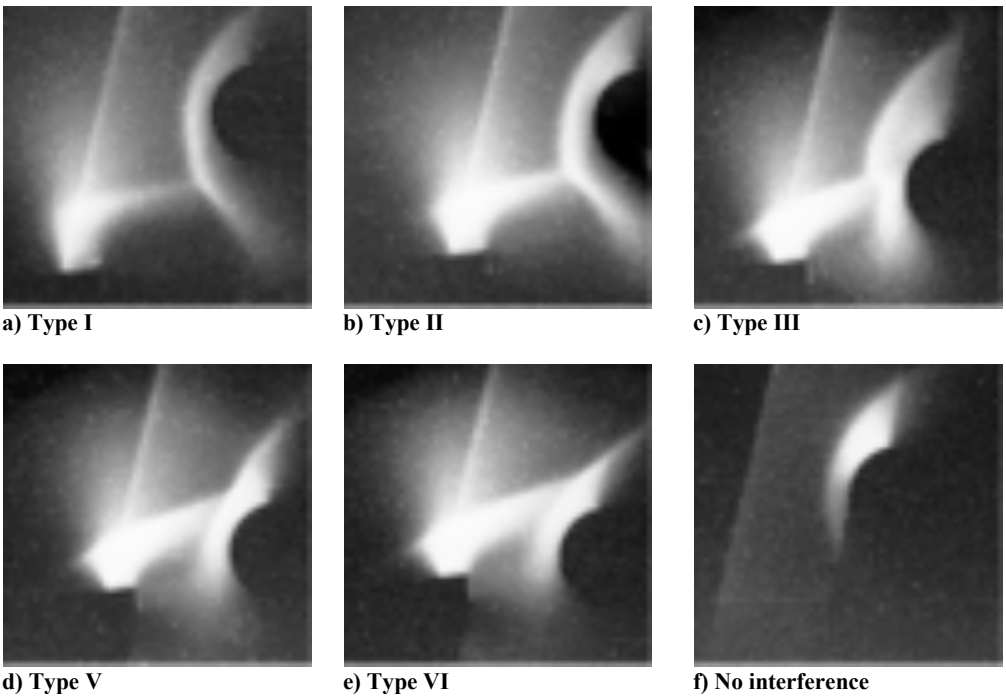

FIGURE 1. Visualization of different type interactions by electron-beam fluorescence at $Re_{R,0} = 15.5$ ($Kn_{R,\infty} = 0.1$): a) type I, b) type II, c) type III; d) type V, e) type VI, and f) no interference.

EXPERIMENTAL TECHNIQUES AND RESULTS

The experiments have been carried out in a vacuum wind tunnel at low-density uniform airflow parameters: $M_\infty = 6.5$, $T_0 = 1000$ K, $p_0 = 4000$ N/m^2, and $t_w = 0.31$. The model is a plate with a cylindrical edge of radius $R = 0.01$ m. The flow can be characterized by similarity parameters: the Reynolds number $Re_{R,0} = 15.5$ and the Knudsen number $Kn_{R,\infty} = 0.1$.

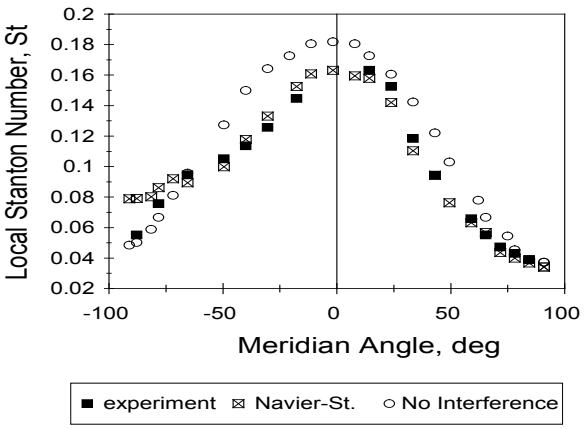

a) Type I

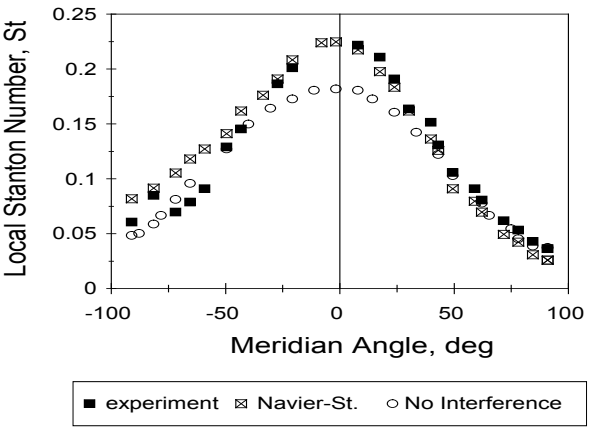

d) Type V

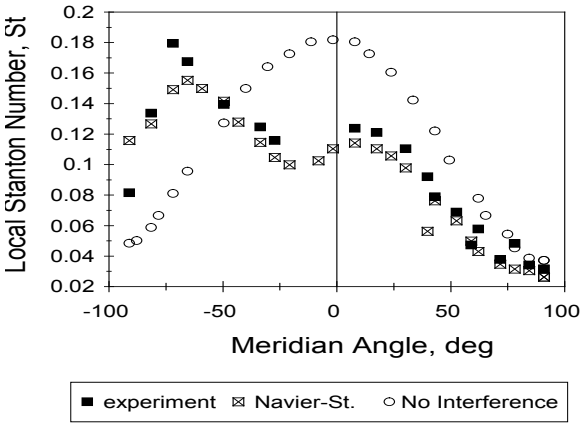

b) Type II

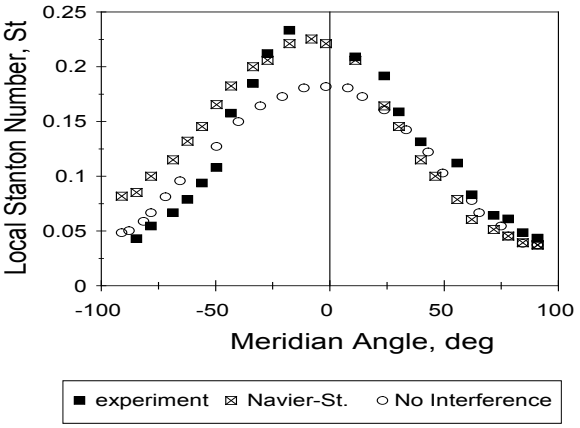

e) Type VI

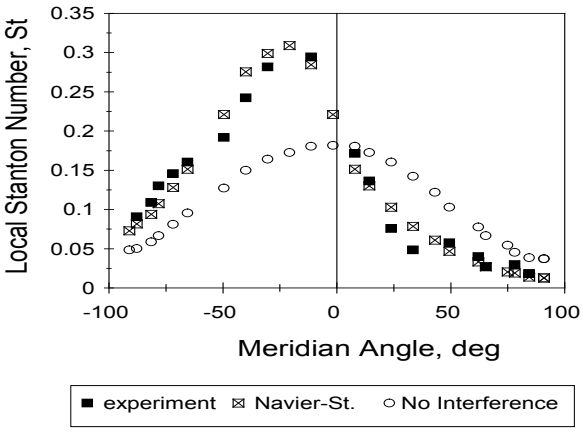

c) Type III

FIGURE 2. Comparison between experimental and numerical results of local Stanton number ratio distributions around a cylinder at $Re_{R,0} = 15.5$ ($Kn_{R,\infty} = 0.1$) for different types of shock/shock layer interference: a) type I; b) type II; c) type III; d) type V, and e) type VI.

The plane oblique shock wave was generated by a wedge with an apex angle $\theta = 20$ deg, and the resulting shock inclination angle β was approximately 27 deg. A string transverse mechanism was used to place the wedge at various positions along the Y-axis to simulate the different interaction patterns.

The electron-beam fluorescence technique [11] was used for flow visualization. Five different cases of interference were found in the experiments (see Figs. 1a–1e corresponding to types I, II, III, V, and VI). The flow patterns were compared with the flow near the cylinder without interference as presented in Fig. 1f.

The local heat flux to the model surface elements was measured using the mono-layered thermal sensitive coating technique [11, 17]. The accuracy of the heat-flux data was studied in detail by Ardasheva et al [17]. The data errors are estimated to be approximately 20 to 40 percent, with the larger errors occurring in the strong interaction. The distributions of the local Stanton number ratios St/St_0 are shown in Figs. 2a–2e for the five types of shock-waves interactions and compared with the numerical results.

THE SOLUTIONS OF THE NAVIER-STOKES EQUATIONS

The system of Navier-Stokes equations, analogous to that presented in Refs. 11, 15, and 18 have been solved numerically. The meridian angle φ is varied over the interval $-90 \le \varphi \le +90$ deg. The steady-state equations in the arbitrary curvilinear coordinate system $\xi = \xi(x, y)$, $\eta = \eta(x, y)$, where x and y are Cartesian coordinates, have been written in the conservation form [11, 15, 18].

The equations have been nondimensionalized with respect to the parameters of free-stream velocity, density, temperature and viscosity. The cylinder radius R is used as a characteristic length scale parameter. The main similarity parameters are the Reynolds number $Re_{R,0}$, Mach number M_∞, the specific heat ratio γ, and the temperature factor t_w.

The outer boundary is divided into two parts: one part with uniform free-stream conditions at the constant Mach number M_∞, and the other with the conditions behind an inclined plane shock [19] (see Fig. 3). The velocity slip and temperature jump effects [20] are considered at the body surface.

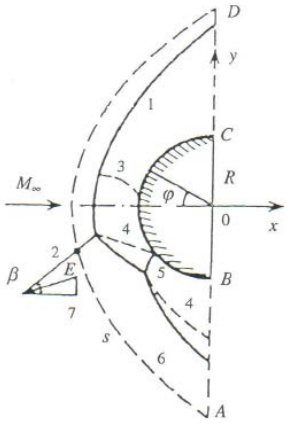

NOTATION:
1 – The boundary of shock layer;
2 – The inclined shock;
3 – The sonic line;
4 – The mixing layer;
5 – The inner shock;
6 – The calculation domain for the Navier-Stokes equations;
7 – The wedge.

NOTE: This pattern is for the Type- III interference.

FIGURE 3. The general flow pattern and calculation domain used by the Navier-Stokes solver.

The numerical method has been described in detail in Refs. 11, 15, and 18. A set of FORTRAN standardized programs [18] has been used to solve the problem. The grid contains 44 nodes related to the surface curvilinear coordinate ξ and 41 nodes along the normal η. The finite-difference program is a second-order accuracy scheme.

THE DIRECT SIMULATION MONTE-CARLO (DSMC) METHOD AND COMPUTATIONAL PARAMETERS

The DSMC method [14] and DS2G code [16] are used in this study as a numerical simulation technique for low-density gas flows. Molecular collisions in air are modeled using the variable hard sphere molecular model [14]. The gas-surface interactions are assumed to be fully diffusive with full momentum and energy accommodation. The code

validation [1, 21] was tested in comparing numerical results with experimental data [22] related to the simple-shape bodies.

For the DSMC calculations, the computational domain was subdivided into six zones with a total of 8400 cells, where the cells were populated with an average of 7 molecules per cell (see Fig. 4). Acceptable results are obtained for an average of at least ten molecules per cell in the most critical region of the flow [14, 21]. The error was pronounced when this number falls below five (i.e., in the flow behind the cylinder). In all cases, the usual criterion [16] for the time step Δt_m has been realized, $2\times10^{-7} \le \Delta t_m \le 1\times10^{-6}$ s. Under these conditions, heat flux, aero-dynamic coefficients, and gas-dynamic parameters are insensitive to the time step.

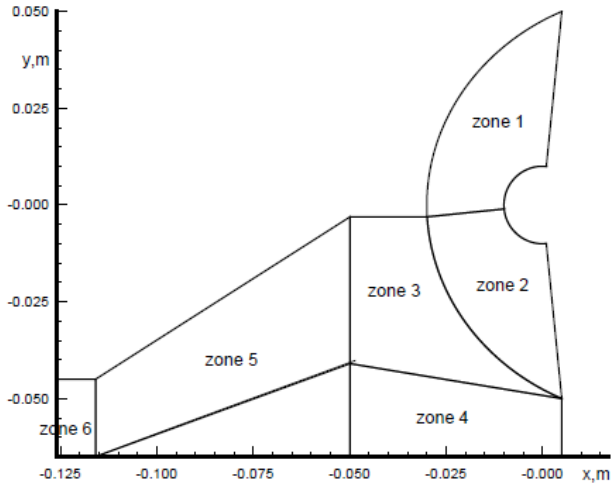

FIGURE 4. The calculation domain used by the DSMC solver.

The location of the external boundary with the upstream flow conditions varies from 2.5R to 3.5R. Calculations were carried out on a personal computer. The computing time of each variant was 10 - 60 h.

RESULTS AND DISCUSSION

The numerical results obtained with the Navier-Stokes technique are presented in Figs. 2a-2e in the form of a distribution of Stanton number ratio St/St_0 values along the cylindrical surface. Five (types I, II, III, V, and VI) of the six known types of interference patterns described in Refs. 5-9 and 12 have been found for the current rarefied air-flow conditions ($Re_{R,0} = 15.5$; $Kn_{R,\infty} = 0.1$; $M_\infty = 6.5$; $\gamma = 1.4$; $T_0 = 1000$ K; $t_w = 0.31$; $\theta = 20$ deg, and $\beta = 27$ deg).

Mach number contours obtained by the DSMC technique under the same airflow conditions are shown in Figs. 5a-5c below for Types II, III, and V interactions. The similar contours obtained with the Navier-Stokes equations were studied in [11].

Heating results for the type I interference are shown in Fig. 2a. The stagnation point has almost returned to its position in the absence of interference. Inhomogeneities of the shock wave or mixing layer type have not been found in the shock layer. The heat transfer coefficient distribution also tends to the distribution obtained in the absence of interference.

Computed and measured heating distributions for the type II interference are shown in Fig. 2b. This type of interaction is observed when the oblique shock impinges on the supersonic region of the shock layer below the regular stagnation line. At high Reynolds numbers, a subsonic jet, bounded by the surfaces of the mixing layers departing from the lower and upper triple points, is formed within the supersonic flow in the shock layer [10]. An inner shock also departs from the upper triple point, crossing the shock layer to the surface of the cylinder. At high Reynolds numbers, this shock produces a sharp increase in the pressure and heat flux to the surface of the blunt body in the zone of impingement.

At moderate Reynolds numbers, visualization [7] and analysis of numerical data do not reveal inner shocks and mixing layers in the viscous shock layer. Only the change of shock layer configuration related to the type II interference has been observed (see Fig. 5a). The stagnation point is displaced significantly downwards along the surface coordinate. In the vicinity of the stagnation point, both in the calculations [11, 13] and in the experiments [7],

the local heat flux has a maximum value. However, the heating values are smaller than the corresponding values for types III, V, and VI interactions.

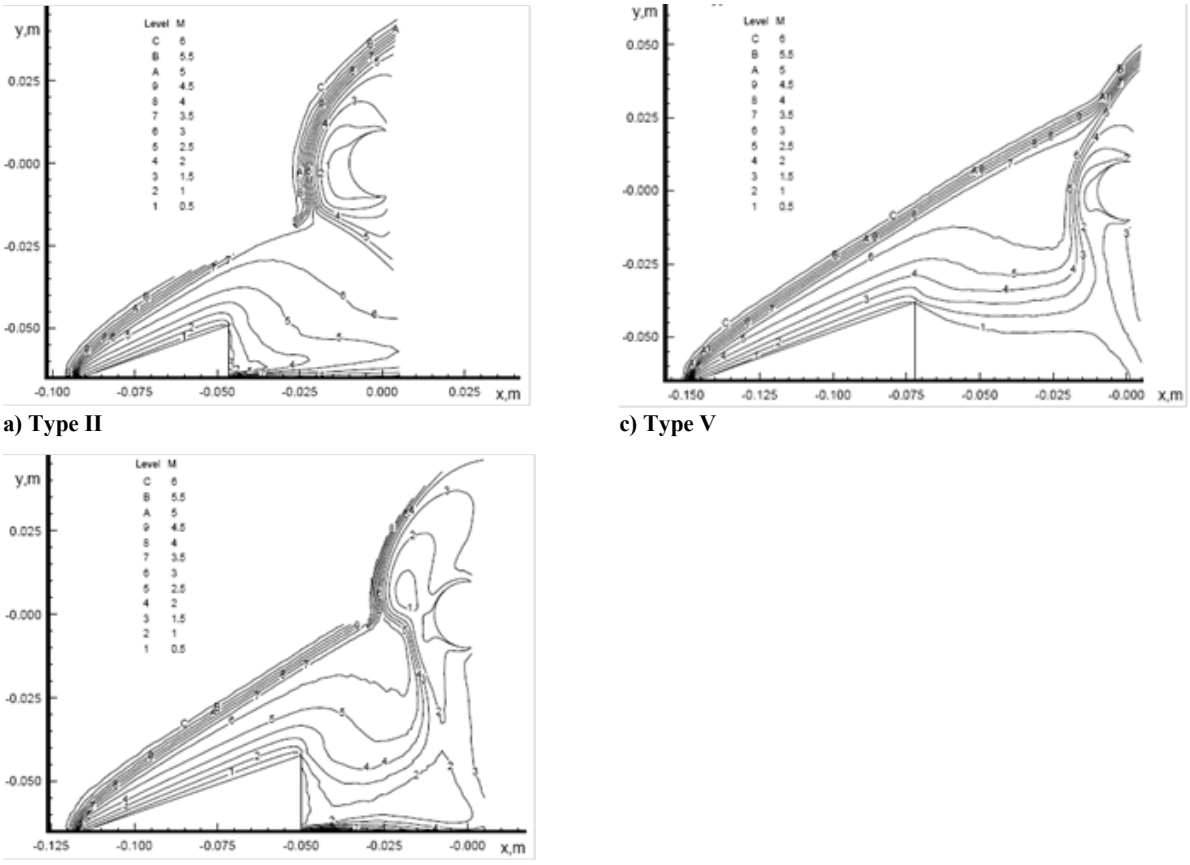

FIGURE 5. Mach number contours calculated by the DSMC technique at $Re_{R,0} = 15.5$ ($Kn_{R,\infty} = 0.1$) for different types of interaction: a) type II, b) type III, and c) type V.

Figure 2c presents the surface heating distributions for the type III interference. According to Refs. 5, 8, and 10, the type III interference occurs when the inclined shock intersects the part of the bow shock almost normal to the free-stream velocity vector. The calculated Mach number contours for the type III interference are presented in Fig. 5b. Experimental data [7, 8] and analysis of the contours indicate that a secondary thick shock originates from the lower triple point towards the body surface. However, the mixing layers are weakly expressed for the current rarefied flow conditions.

According to the study of Tannehill, Holst, and Rakich [10], at high Reynolds numbers, the maximum pressure and heat flux values correspond to the region where the secondary shock impinges on the boundary layer (the type III interference). At moderate Reynolds numbers, it has been found [11] that the maximum values of the heat flux are attained not in the surface-secondary-shock interaction zone but, as before, in the vicinity of the stagnation point displaced in the direction of negative φ. In this flow regime, the greatest increase in the maximum value of the heat flux is observed as compared with regular flow without interference (see Fig. 2c).

At high Reynolds number conditions, the type IV interference [6-10, 23] produces the maximum pressure and heat flux. In our study, the type IV interference is not found. At low Reynolds numbers, it appears that no supersonic jet is formed. This result occurs because the shock layer is completely viscous, and the mixing-layer boundaries and the inner shocks in the viscous shock layer are thick. Therefore, as the wedge is displaced downward along the Y-axis, the type V interference becomes a type III interference, by-passing type IV.

Substantial differences are observed between the flow patterns for the type V interference at high Reynolds numbers [7, 10] and the low Reynolds numbers in this study. The cause of the local increase in the pressure and the

heat flux to the body surface at high Reynolds numbers is the interaction between the secondary shock passing through the bow shock wave and the boundary layer on the body. At low Reynolds numbers the entire region from the bow shock to the body is a thick viscous shock layer. In this case, the secondary shock dissipates in the shock layer and no longer causes a local increase in the pressure and the heat flux to the surface. No secondary shock was observed in the experiments [11, 13].

The calculated Mach number contours for the type V interference are presented in Fig. 5c, using the DSMC approach. Significant changes of the flow structure can be observed in the area below the shock intersection point. The level of air compression in this zone is much higher than behind the bow shock wave in the absence of interference. The interaction increases the heat flux by approximately 20% near the leading stagnation point (see Fig. 2d).

Figure 2e shows the type VI interference that results when the oblique shock impinges on the upper supersonic region of the shock layer at a sufficient distance from the stagnation point. Behind the interference zone, the shock layer thickness increases significantly because the flow behind the oblique shock affects almost the entire region in front of the blunt body. This leads to a redistribution of the flow parameters in the shock layer and to a change in its structure. The stagnation point is displaced into the region of negative φ. In the vicinity of this point there is a significant increase in the values of the local heat flux. The calculated results are compared with experimental data [11] (solid rectangles) and the distributions of the calculated values of the local Stanton numbers in the absence of interference (dashed line). At $\varphi < -35$ deg, the experimental values of the local heat flux are significantly lower than the calculated values. In experiments provided by the thermal indicator coating method [17], the study region lies in the wake of expanding flow from the wedge trailing edge. This feature is also present, although to a smaller extent, in Fig. 2d, which corresponds to the type V interference.

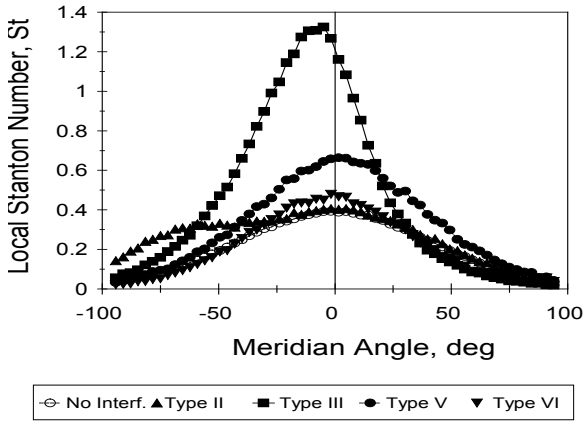

a) Local Stanton number

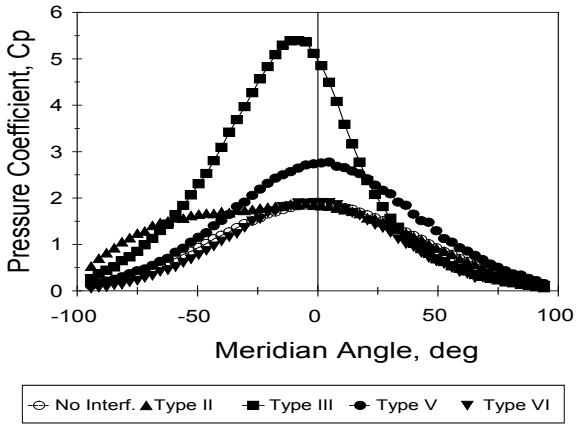

c) Local skin friction coefficient

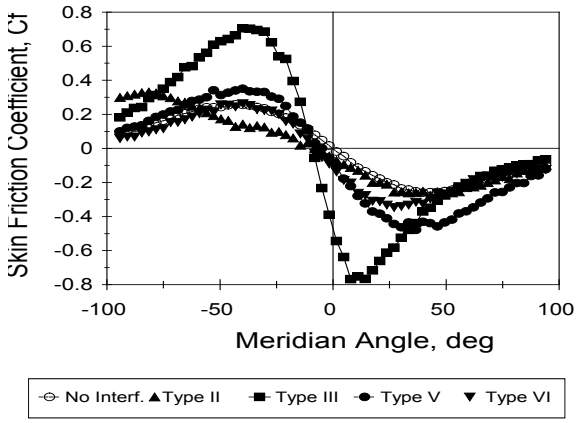

b) Local pressure coefficient

FIGURE 6. Distributions of local flow parameters on the cylinder surface at Reynolds number $Re_{R,0} = 15.5$ ($Kn_{R,\infty} = 0.1$) for different interference types.

The DSMC results on distributions of the heat, pressure and local skin-friction coefficients for this flow regime and different types of interference at $Kn_{R,\infty} = 0.1$ ($Re_{R,0} = 15.5$) are shown in Figs. 6a, 6b, and 6c, respectively.

RESULTS FOR THE MODERATE REYNOLDS NUMBERS

Numerical data obtained by the DSMC technique have been studied at the near-continuum free-stream conditions of rarefied air ($Re_{R,0} = 124$; $Kn_{R,\infty} = 0.012$; $M_\infty = 6.5$; $T_0 = 1000$ K; $t_w = 0.31$, and $\theta = 20$ deg). Mach number contours and streamlines are shown in Figs. 7a and 7b, respectively, for the type III interaction. Thickness of the oblique and bow shocks becomes smaller in comparison with the corresponding results for the more rarefied condition ($Kn_{R,\infty} = 0.1$). The effective angle of the oblique shock becomes smaller because of the thinner boundary layer along the wedge surface.

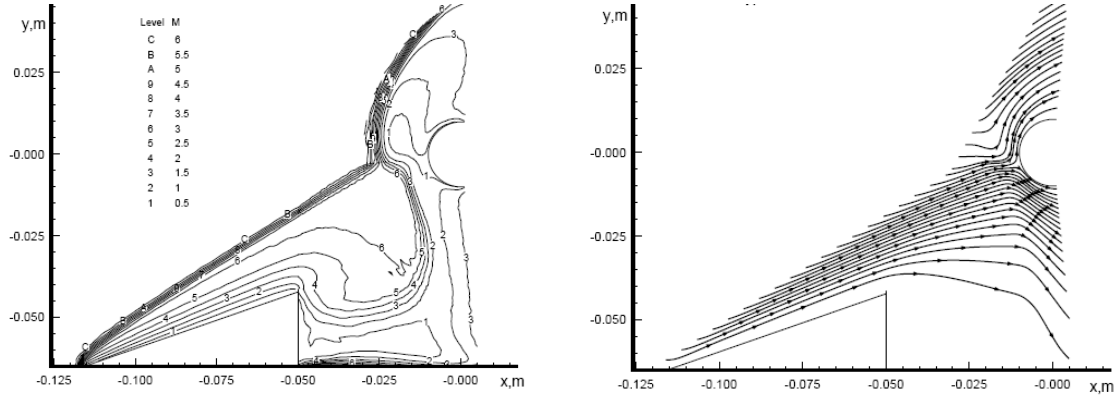

a) Mach number contours **b) Streamlines**

FIGURE 7. Mach number contours and streamlines calculated by the DSMC technique at $Re_{R,0} = 124$ ($Kn_{R,\infty} = 0.012$) for the type III interaction.

The latest phenomenon is pronounced significantly for the type III interference. It results in moving down the actual stagnation point, which is identified from distributions of heat, pressure, and skin friction (see Figs. 8a, 9a, and 10a). For other interference types this phenomenon is not pronounced (e.g., see Figs. 8b, 9b, and 10b for the type II interference).

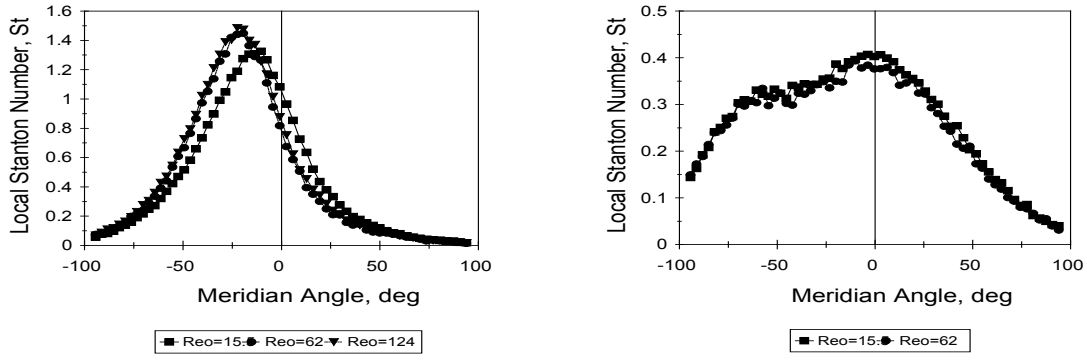

a) Type III **b) Type II**

FIGURE 8. Local Stanton number distributions around a cylinder at various Reynolds numbers $Re_{R,0}$ for different types of shock/shock-layer interference: a) type III; b) type II.

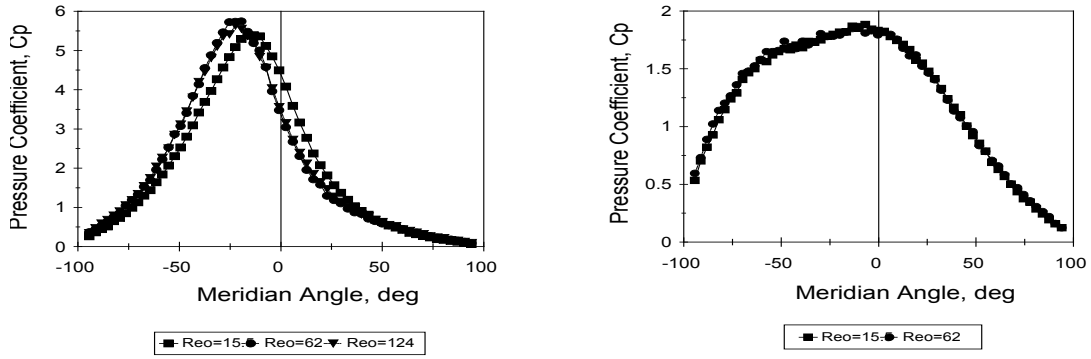

a) Type III **b) Type II**

FIGURE 9. Local pressure coefficient distributions around a cylinder at various Reynolds numbers $Re_{R,0}$ for different types of shock/shock-layer interference: a) type III; b) type II.

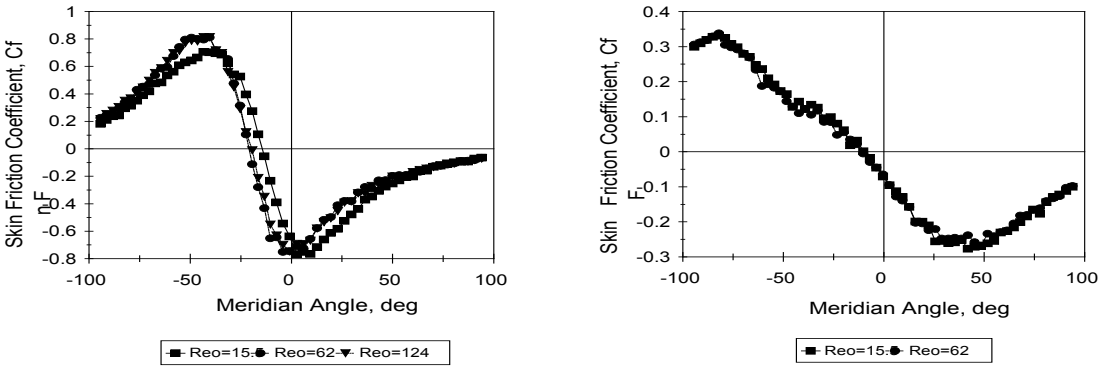

a) Type III **b) Type II**

FIGURE 10. Local skin friction coefficient distributions around a cylinder at various Reynolds numbers $Re_{R,0}$ for different types of shock/shock-layer interference: a) type III; b) type II.

CONCLUDING REMARKS

The different types of interference between the impinging plane oblique shock wave and the shock layer near a cylinder have been studied at low and moderate Reynolds numbers. It has been found that the type IV interference (reported in [23]) does not take place under the transitional flow regimes studied here experimentally and computationally using both the direct simulation Monte-Carlo technique and the Navier-Stokes equations. Interference of this type occurs only at higher Reynolds numbers $Re_{R,0}$, when the inclined shock impinges on the part of the bow shock almost perpendicular to the free-stream velocity vector. In this case, the gas passing through the system of oblique secondary shocks forms a supersonic jet, in which the total pressure is much higher than in the surrounding subsonic flow. For types VI, V, and III interference patterns, the maximum pressure and heat flux parameters on the cylinder surface are considerably greater than the values in the absence of interference. This fact is in a good agreement with known experimental and analytical results.

REFERENCES

1. V. V. Riabov, J. Spacecr. Rockets **39**(6), 910-916 (2002).
2. V. V. Riabov and A. V. Botin, "Shock Interference in Hypersonic Rarefied-Gas Flows Near a Cylinder," AIAA Paper No. 99-3207, Washington, DC, USA, June 1999.
3. F. S. Billig, J. Propuls. Power **9**(4), 499-514 (1993).
4. V. N. Gusev, Fluid Dyn. **28**(2), 269-276 (1993).

5. B. Edney, "Anomalous Heat Transfer and Pressure Distributions on Blunt Bodies at Hypersonic Speeds in the Presence of an Impinging Shock," Aeronautical Research Institute of Sweden, FFA Report 115, Stockholm, Sweden, 1968.
6. A. R. Wieting and M. S. Holden, AIAA J. **27**(11), 1557-1565 (1989).
7. V. Ya. Borovoi, *Gas Flow and Heat Transfer in Shock Wave-Boundary Layer Interaction Zones* (Mashinostroenie, Moscow, Russia, 1983) (in Russian).
8. V. Ya. Borovoi, A. Yu, Chinilov, V. N. Gusev, I. V. Struminskaya, J. Délery, and B. Chanetz, "Interference Between a Cylindrical Bow Shock and a Plane Oblique Shock," AIAA Paper No. 96-2374, Washington, DC, USA, June 1996.
9. C. Purpura, B. Chanetz, J. Délery, and F. Grasso, "Type III and Type IV Shock/Shock Interferences: Theoretical and Experimental Aspects," in *Rarefied Gas Dynamics*, Proceeding of the 21st International Symposium on Rarefied Gas Dynamics, Part I (Cépadeuś-Éditions, Toulouse, France, 1998), pp. 21-28.
10. J. C. Tannehill, T. L. Holst, and J. Rakich, AIAA J. **14**(2), 204-211 (1976).
11. A. V. Botin, Fluid Dyn. **28**(1), 126-130 (1993).
12. T. Pot, B. Chanetz, M. Lefebvre, and P. Bouchardy, "Fundamental Study of Shock/Shock Interference in Low Density Flow: Flowfield Measurements by DLCARS," in *Rarefied Gas Dynamics*, Proceeding of the 21st International Symposium on Rarefied Gas Dynamics, Part II (Cépadeuś-Éditions, Toulouse, France, 1998), pp. 545-552.
13. V. V. Riabov and A. B. Botin, "Numerical and Experimental Studies of Shock Interference in Hypersonic Flows near a Cylinder," in *Proceedings of the 26th International Congress of the Aeronautical Sciences*, Paper No. 71, Anchorage, AL, USA, 2008, pp. 1-10.
14. G. A. Bird, *Molecular Gas Dynamics and the Direct Simulation of Gas Flows* (Oxford University Press, Oxford, UK, 1994).
15. I. V. Egorov and O. L. Zaitsev, J. Comput. Math. Mathem. Phys. **31**(2) 286-299 (1991).
16. G. A. Bird, *The DS2G Program User's Guide, Version 3.2* (Killara, Australia, 1999).
17. M. Ardasheva, T. V. Klimova, G. V. Pervushin, and L. G. Chernikova, Trudy TsAGI **2111**, 197-207 (1981) (in Russian).
18. I. V. Yegorov, M. V. Yegorova, D. V. Ivanov, and V. V. Riabov, "Numerical Study of Hypersonic Viscous Flow About Plates Located Behind a Cylinder," AIAA Paper No. 97-2573, Washington, DC, USA, June 1997.
19. J. D. Anderson, Jr., *Hypersonic and High Temperature Gas Dynamics* (McGraw-Hill, New York, NY, 1989).
20. M. N. Kogan, *Rarefied Gas Dynamics* (Plenum Press, New York, NY, 1969).
21. V. V. Riabov, J. Spacecr. Rockets **35**(4), 424-433 (1998).
22. V. N. Gusev, A. I. Erofeev, T. V. Klimova, V. A. Perepukhov, V. V. Riabov, and A. I. Tolstykh, Trudy TsAGI **1855**, 3-43 (1977) (in Russian).
23. J. N. Moss, T. Pot, B. Chanetz, and M. Lefebvre, "DSMC Simulation of Shock/Shock Interactions: Emphasis on Type IV Interaction," in *Proceedings of the 22nd International Symposium on Shock Waves*, Vol. 3570 (Imperial College, London, UK, 1999), pp. 1337-1342.